Optics & Laser Technology 63 (2014) 19–23

Contents lists available at ScienceDirect

Optics & Laser Technology

journal homepage: www.elsevier.com/locate/optlastec

Temperature dependent polarization switch of 850-nm VCSELs with different apertures

Qiang Wang [a], Baolu Guan [a,b,*], Ke Liu [a], Xin Liu [a], Xiaowei Jiang [a], Yunhua Ma [a], Shamsul Arafin [b], Guangdi Shen [a]

[a] *Key Laboratory of Opto-electronics Technology, Ministry of Education, Beijing University of Technology, Beijing 100124, China*
[b] *Electrical Engineering Department, University of California at Los Angeles, CA 90095, United States*

ARTICLE INFO

Article history:
Received 25 November 2013
Received in revised form
26 February 2014
Accepted 2 March 2014
Available online 10 April 2014

Keywords:
Vertical-cavity surface-emitting lasers
Temperature dependent polarization switch
Different apertures

ABSTRACT

Temperature greatly affects the polarization properties of VCSELs. In this paper, these polarization properties of top-emitting 850-nm VCSELs are simulated by numerical calculation and then they are verified by experimental measurement. For a 4-μm aperture VCSEL, polarization switch current reduces from 1.4 mA to 0.4 mA as the temperature increases from 273 K to 323 K, which is caused by the change of the reflectivity of DBR and differential gain for LP_{01} transverse-mode. For VCSELs with 8-μm aperture, the first polarization switch current reduces from 2.1 mA to 0.8 mA as temperature increases from 273 K to 313 K. However, the second polarization switch current increases from 3.8 mA to 6.3 mA for the same increase in temperature because of the competition and polarization selection among several higher-order transverse modes. When the device aperture is further increased to 12 μm or 16 μm, there are several high-order transverse modes emitting even at small injection current, resulting in a serious competition and selection among themselves. This is why the polarization characteristics of VCSELs with 12 μm or larger aperture are irregular and different from those of smaller aperture devices. Our research results provide useful guidelines for the application of VCSELs operating at different ambient temperatures.

1. Introduction

Vertical-cavity surface-emitting laser (VCSEL) is a promising light source in many applications, such as spectroscopy, optical communication and optical interconnects [1–4]. And the polarization performance of VCSEL is an important characteristic which influences its applications and development. For example, data communication greatly promotes development of the VCSEL technology [5]. However, the polarization instability increases the noise intensity, which reduces the signal-to-noise ratio of the optical system, thereby degrading the link quality [6]. In the spectroscopy application, the polarization instability will change the contrast ratio of optical power of the orthogonal polarization light and enlarge the measuring error [7]. In the air detector, the polarization instability will change the emitting wavelength and lower the detection accuracy [8]. Therefore, extensive efforts have been devoted to study the thermal characteristics of VCSEL for avoiding temperature instability. There are many ways to avoid the polarization instability of VCSEL, such as high contrast grating [9], asymmetric current injection [10], asymmetric oxide aperture [11], selective epitaxy [12], etc.

In this paper, we study the characteristics of a temperature dependent polarization switch. When temperature increases, the refractive index of $Al_xGa_{1-x}As$ changes simultaneously. The reflectivities of distributed Bragg reflector (DBR) for the linear polarized (*LP*) mode aligning $[0\bar{1}1]$ and [011] crystal orientation are different and change as the temperature increases. With a change in temperature, differential gain will simultaneously change. Here, we define the *LP* mode aligning [011] and $[0\bar{1}1]$ as *H-LP* mode and *L-LP* mode, respectively. From calculation, we find that the temperature affects the optical power of two orthogonal polarized lights. From the experiment, for the single mode emitted by VCSELs with a 4-μm aperture, the polarization switch (*PS*) current reduces from 1.4 mA to 0.4 mA as temperature increases from 273 K to 323 K. However, for a device with an 8-μm aperture, there are several higher-order transverse-modes which greatly influence the *PS* current. The first *PS* current reduces from 2.1 mA to 0.8 mA as temperature increases from 273 K to 313 K. However, the second *PS* current increases from 3.8 mA to 6.3 mA for the same increase in temperature. For comparison, we measured the temperature dependent polarization and spectrum characteristics of the VCSELs with 12-μm and 16-μm apertures. From the experimental results, we find that the light–current curves are not formed because of serious modes of competition and selection among higher-order transverse-modes.

* Corresponding author. Tel.: +86 10 67391641 812.
E-mail address: gbl@bjut.edu.cn (B. Guan).

http://dx.doi.org/10.1016/j.optlastec.2014.03.001
0030-3992/

2. Device structure and fabrication process

Fig. 1 illustrates the device schematic of a VCSEL. The VCSEL structure was grown on n-doped GaAs-substrate by MOCVD. A 20/34 periods doped $Al_{0.12}Ga_{0.88}As/Al_{0.90}Ga_{0.10}As$ DBR with 20 nm thick linear graded interfaces was employed for the top/bottom reflector. The active region contains three 7.2 nm thick GaAs QWs with 8 nm thick $Al_{0.30}Ga_{0.70}As$ barrier layers. For current and optical confinement, the $Al_{0.98}Ga_{0.02}As$ layer was placed above the active region.

A circular mesa was etched deep enough to expose the $Al_{0.98}Ga_{0.02}As$ layer. Then we utilized wet oxidation technology to form aluminum oxide aperture of 4 μm/8 μm by oxidizing the $Al_{0.98}Ga_{0.02}As$ layer. After that, Ti–Au and Au–Ge–Ni–Au were deposited and annealed as top injection electrode and bottom electrode, respectively.

3. Results and discussion

Fig. 2 shows the experimental setup for *I–P* characteristics of VCSEL which consists of the laser driver (LD), the Peltier temperature controller (PTC) and the photodetectors (D). On the VCSEL probe station, *H-LP* and *L-LP* modes are separated by the polarization beam splitter (PBS). The photodetectors will receive the optical signal and transfer it to the computer in order to obtain the polarization dependent *I–P* curves. The Peltier temperature controller is used to control the temperature of heater.

For a single mode VCSEL operating in *H-LP* mode [13]

$$[v_{gH}g_H\varepsilon_s]P_H^2+\left[-\tau_p^H\Gamma v_{gH}g_H\varepsilon_s\left(\frac{\eta J}{ed\pi s^2}-\frac{N_{tr}}{\tau_e}\right)-v_{gH}g_H\right]P+\left[\tau_p^H\Gamma v_{gH}g_H\left(\frac{\eta J}{ed\pi s^2}-\frac{N_{tr}}{\tau_e}\right)-\frac{1}{\tau_e}\right]=0 \quad (1)$$

Here, v_{gh} and g_H are, respectively, the group velocities and the differential gains for *H-LP* mode, ε_s is the self-compression coefficient, P_H is the power of *H-LP* mode, Γ is the confinement factor, η is the current injection efficiency, J is the injection current, d is the active region thickness, s is the radius of the VCSEL aperture, N_{tr} is the carrier density at transparency, and τ_e is the carrier lifetime. The τ_p^H can be expressed as follows [13]:

$$\tau_P^H=\frac{n^H}{C}\left[\alpha_{\rm int}+\frac{1}{L_c}\ln\left(\frac{1}{\left|r_{top}^H r_{bottom}^H\right|}\right)\right]^{-1} \quad (2)$$

Utilizing the parameters, $\tau_e=1$ ns, $d=0.032$ μm, $\eta=0.7$, $g_{H(L)}=8(8.013)*10^{-8}\,\mu m^2$, $dn/dJ=3\times10^{-3}\,mA^{-1}$, $s=2\,\mu m$, $\alpha_{int}=0.005\,\mu m^{-1}$, $L_c=1.4865\,\mu m$, $\varepsilon_{s(c)}=2.5(5)\times10^{-7}\,\mu m^3$, $N_{tr}=4\times10^6\,\mu m^{-3}$, $dg_{H(L)}/dJ=-1(-2)10^{-10}\,\mu m^2\,mA^{-1}$, $n_0^{H(L)}=3.406(3.40609)$, we obtain the *I–P* curve of *H-LP* mode by solving the second-order equation(1). Then by replacing *H* with *L*, we can obtain the *I–P* curve of *L-LP* mode. These two *I–P* curves will have a cross point, namely *PS* point, greatly dependent on the temperature. The *PS* current of VCSEL is expressed as [13]

$$J_i=\frac{ed\pi s^2}{\eta}\left[\frac{N_{tr}}{\tau_e}+\frac{1-\frac{r_j}{r_i}}{\Gamma\tau_p^j(\varepsilon_s+\varepsilon_c)}+\frac{r_i}{\Gamma\tau_e(\varepsilon_s-\varepsilon_c)}\right] \quad (3)$$

$$r_i=\frac{\varepsilon_s}{v_{gi}g_i\tau_p^i}-\frac{\varepsilon_c}{v_{gj}g_j\tau_p^j} \quad (4)$$

Here, $i=H,L(j=L,H)$.We can describe the *I–P* curves shown in Fig. 3 as follows. When the ambient temperature is room temperature (303 K), the *PS* current is 1.13 mA. When the injection current is smaller than that of the *PS*, the *H-LP* mode is the only optical output. On the contrary, when the injection current is larger, the *L-LP* mode light has priority to emit.

In VCSELs, the *PS* current is mainly influenced by the DBR reflectivity and the differential gain which are also changed by the temperature. Here the change of the DBR reflectivity is caused by the change of the refractive indices of DBR materials which are also functions of temperature [14].

$$\frac{dn}{dT_{GaAs}}=2.67\times10^{-4}/K \quad (5)$$

$$\frac{dn}{dT_{AlAs}}=1.43\times10^{-4}/K \quad (6)$$

$$\frac{dn}{dT_{Al_xGa_{1-x}As}}=x\frac{dn}{dT_{AlAs}}+(1-x)\frac{dn}{dT_{GaAs}} \quad (7)$$

Using the transfer matrix method (TMM) [15]and Eq. (7), we can calculate the DBR reflectivity and its change with temperature. Fig. 4(a) and (b) shows the change of reflectivities of top and bottom DBRs when the temperature increases. The reflectivities in both top and bottom DBRs increase when the temperature changes from 273 K to 323 K. By Eqs. (3) and (4) and material parameters stated above, we can obtain the *PS* current at different

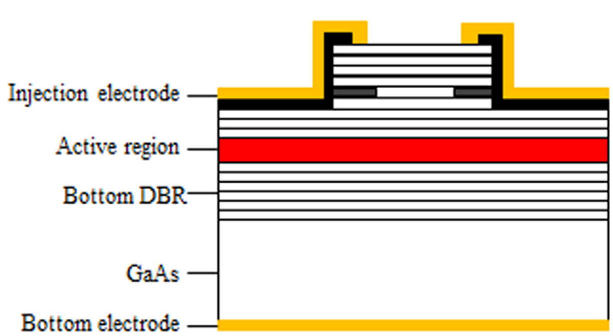

Fig. 1. Structure schematic of 850-nm VCSEL.

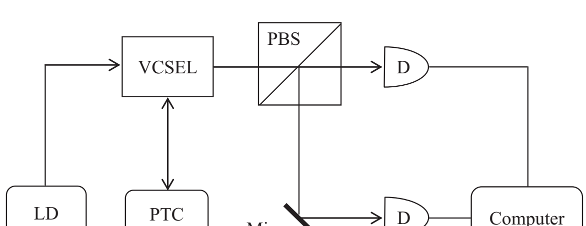

Fig. 2. The examination system of *I–P* characteristics of VCSEL.

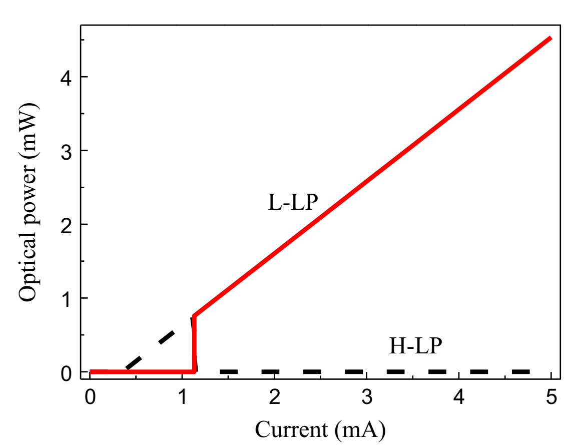

Fig. 3. The *I–P* curves of VCSEL at 303 K.

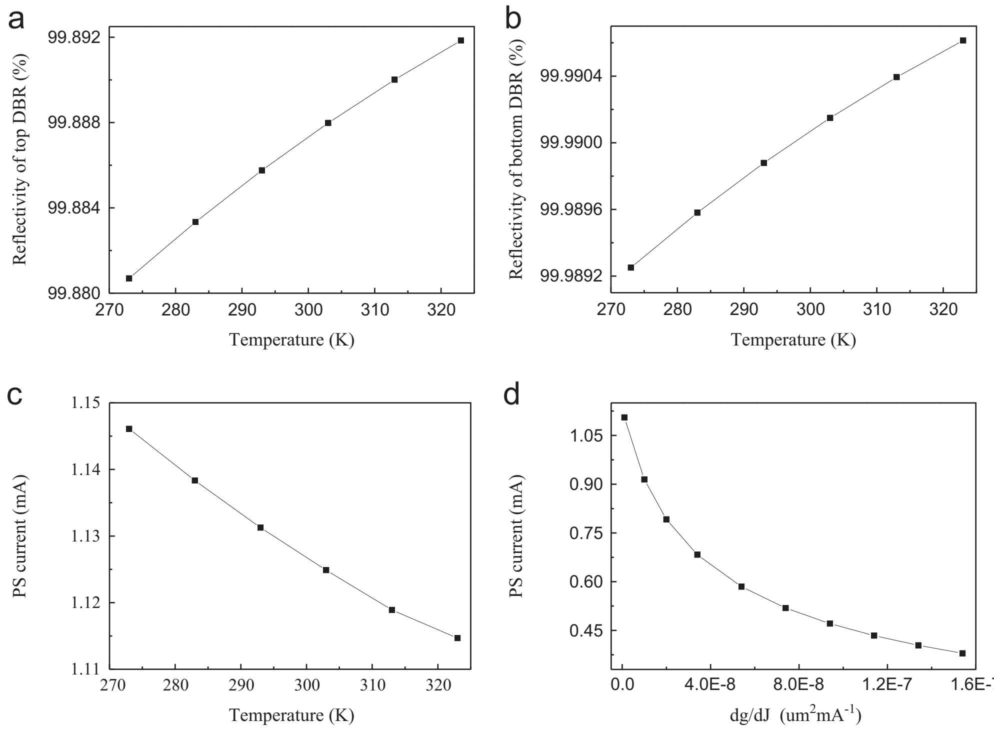

Fig. 4. The reflectivity of (a) top DBR and (b) bottom DBR, (c) temperature dependent PS current (only reflectivity change considered) and (d) differential gain changes the PS current when DBR reflectivity is fixed as a constant.

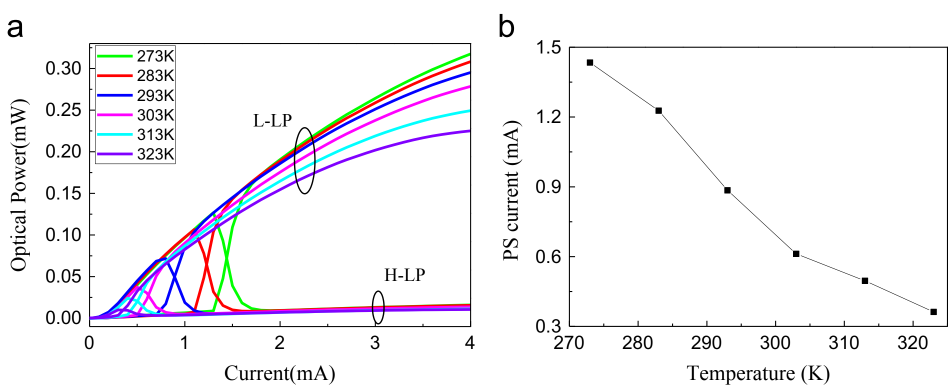

Fig. 5. (a) Temperature dependent polarization *I–P* curves of VCSEL and (b) temperature dependent *PS* currents of VCSEL.

temperatures. Fig. 4(c) shows the change of *PS* current as the temperature increases. When the DBR reflectivity is considered to be the only factor, we can find that the *PS* current reduces from 2.8 mA to 2.4 mA as the temperature increases from 273 K to 323 K.

The differential gain also greatly changes as the temperature increases. For comparison, we fix the reflectivity as a constant and calculate the PS current point by making the differential gain change in an appropriate range [16]. As shown in Fig. 4(d), the *PS* point reduces from 1.13 mA to 0.37 mA as the differential gain increases. These calculation results are well matched to the experiment results given as follows.

Utilizing the test system in Fig. 2, we measure the polarization dependent *I–P* characteristics of VCSEL with aperture of 4 μm at different temperatures. And Fig. 5(a) shows the temperature dependent *I–P* curves for *H/L-LP* of VCSEL. Fig. 5(b) shows the *PS* current of VCSEL with 4-μm aperture at different temperatures. The *PS* current decreases from 1.4 mA to 0.4 mA as the temperature increases from 273 K to 323 K. Both the reflectivity of DBR and the differential gain analyzed above lead to the experimental results.

The 4-μm aperture is small enough to form a single mode, and the *PS* phenomenon is obvious [17]. However, when aperture increases, there are multi-transverse modes emitting and polarization state becomes complex [18]. Namely, the polarization state is the coexistence of multi-transverse modes. Transverse-mode competition and polarization selection greatly affect the polarization properties. Temperature dependent *PS* current will not follow the law stated above. For example, when the aperture is 8 μm, we measure the polarization dependent *I–P* curves at different temperatures. Fig. 6shows the condition when the ambient temperature increases from 273 K to 313 K and the first *PS* current reduces from 2.1 mA to 0.8 mA. For single mode at smaller currents, the change of *PS* point is similar to that of the 4-μm aperture. However, the second *PS* current, for multi-transverse modes at larger currents, increases from 3.8 mA to 6.3 mA which is different for the single mode. Fig. 7(a) shows the spectrum of VCSEL with 8-μm aperture at 293 K. The peak wavelength is 850.4 nm and full

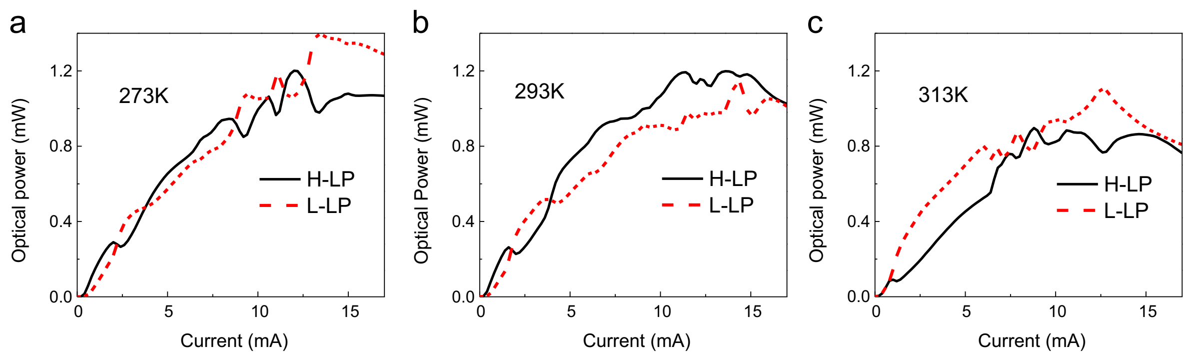

Fig. 6. Polarization dependent *I–P* curves at different temperatures: (a) 273 K, (b) 293 K, and (c) 313 K.

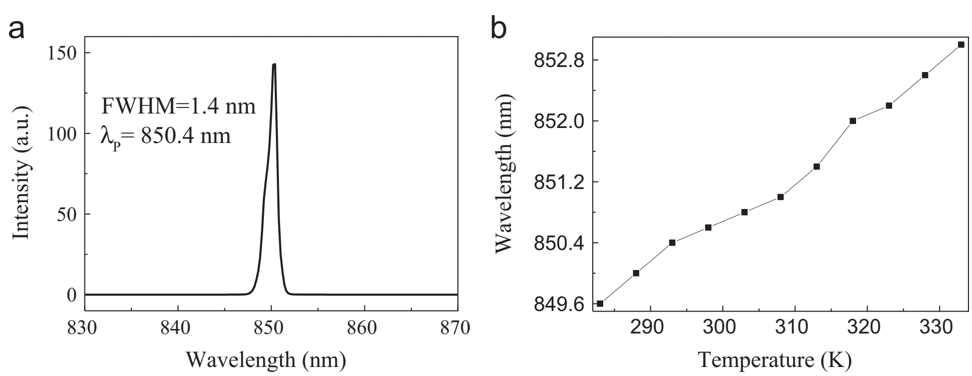

Fig. 7. (a) Output spectra of VCSEL with 8-μm aperture at 293 K (b) and temperature dependent peak wavelength.

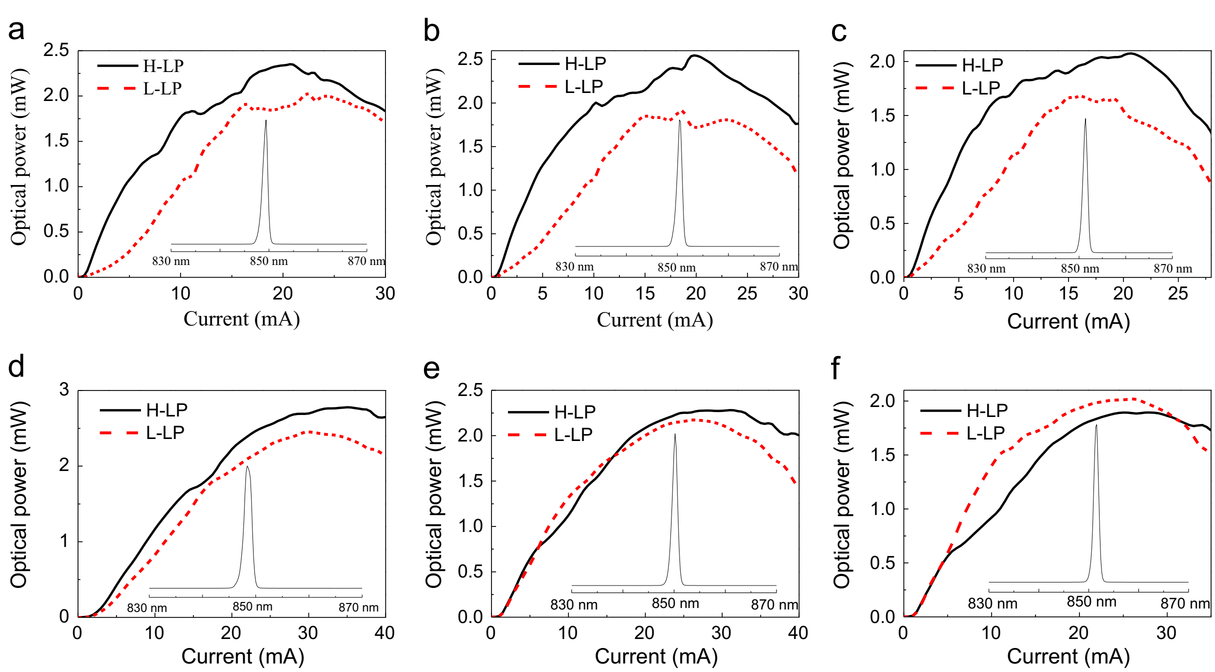

Fig. 8. The polarization dependent *I–P* curves and output spectra of VCSEL: (a) 12 μm, 288 K, (b) 12 μm, 308 K, (c) 12 μm, 323 K, (d) 16 μm, 288 K, (e) 16 μm, 308 mAand (f) 16 μm, 323 K.

width at half maximum (FWHM) is 1.4 nm. From Fig. 7(b), we can find that the peak wavelength red-shifts from 849.6 nm to 853.0 nm when temperature increases from 283 K to 333 K. This is because when temperature increases, both gain spectrum of quantum well and resonant wavelength have a red-shift.

For further study, we measure the polarization dependent *I–P* curves of the VCSEL with 12 μm and 16 μm aperture at different temperatures. Fig. 8shows the *I–P* properties and the lasing spectra of VCSELs with different aperture diameters. As can be seen, the *I–P* curves are not smooth which could be due to the emission of several transverse modes in large aperture VCSELs at a particular injection current. Even though the injection current is small, there are several multi-transverse modes emitting and serious modes competition. Fig. 9 shows the wavelength red-shift of VCSELs. For 12 μm, the wavelength shifts from 849.0 nm to 852.2 nm when the temperature increases from 283 K to 333K. And for 16 μm, the

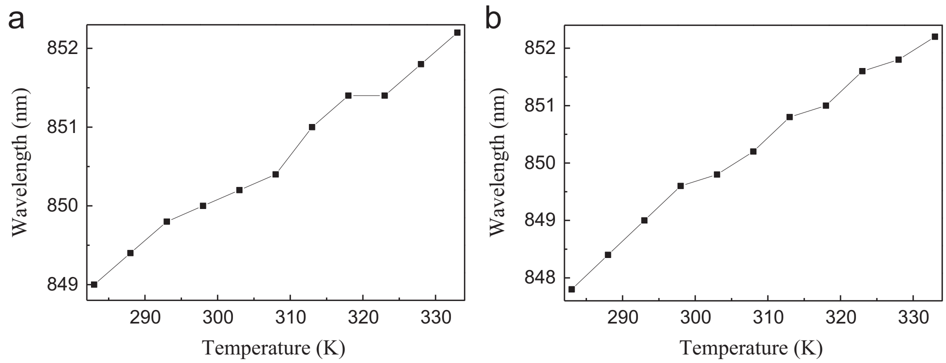

Fig. 9. Temperature dependent wavelength shift of VCSEL with aperture: (a) 12 μm and (b) 16 μm.

wavelength shifts from 847.8 nm to 852.2 nm for the same increase in temperature. The wavelength of VCSEL with 12-μm or 16-μm aperture has a red-shift like 8 μm because of the red-shifts of gain spectrum and resonant cavity.

4. Conclusion

In conclusion, we study the temperature dependent *PS* characteristics of VCSELs with different apertures. When the ambient temperature increases, the temperature sensitive refractive indices of $Al_xGa_{1-x}As$ increase the reflectivities of top and bottom DBRs. Thus the *PS* current changes due to the change of both DBR reflectivity and the differential gain with temperature. For devices with 4-μm aperture, the *PS* current reduces from 1.4 mA to 0.4 mA as the ambient temperature increases from 273 K to 323 K. However, for the 8-μm aperture, there are several transverse-modes that coexist. Transverse-modes competition and polarization selection greatly affect the *PS* current. By measuring experiments, we find that the first (second) *PS* current reduces (increases) from 2.1 (3.8) mA to 0.8 (6.3) mA at smaller (larger) currents as temperature increases from 273 K to 313 K. For larger aperture (12 μm or 16 μm), there are more transverse-modes having competition and polarization selection. Further study of these large aperture VCSELs will be necessary for high power application.

Acknowledgments

This research was supported in part by the National Natural Science Foundation of China under Grant nos.60908012 and 61076148 and Foundation of Beijing Municipal Education Commission under Grant no. KM201010005030.

References

[1] Lackner M, Schwarzott M, Winter F, Kogel B, Jatta S, Halbritter H, Meissner P. CO and CO_2 spectroscopy using a 60 nm broadband tunable MEMS-VCSEL at 1.55 μm. Opt Lett 2006;31:3170–2.

[2] Larsson A. Advances in VCSELs for communication and sensing. IEEE J Sel Top Quantum Electron 2010;17:26–30.

[3] Arafin S, Bachmann A, Kashani-Shirazi K, Markus-Christian A. Electrically pumped continuous-wave vertical-cavity surface-emitting lasers at ~2.6 μm. Appl Phys Lett 2009;95:131120.

[4] Gierl C, Zogal K, Jatta S, Davani H, Küppers F, Meissner P, et al. Tuneable VCSEL aiming for the application in interconnects and short haul systems. Proc SPIE 2011;7959:795908.

[5] Tatum J A. VCSEL proliferation. Proc SPIE 2007;6484:648403.

[6] Nishiyama N, Caneau C, Tsuda S, Guryanov G, Hu M, Bhat R, Zah C. 10-Gb/s error-free transmission under optical reflection using isolator-free 1.3 μm InP-based vertical-cavity surface-emitting lasers. IEEE Photon Technol Lett 2005;17:1605–7.

[7] Michalzik R. J M Ostermann , A Al-Samaneh , D Wahl , F Rinaldi P Debernardi , Polarization-stable VCSELs for optical sensing and communications. In: Proceedings of 14th OECC, 2009 p. 1–2.

[8] Ostermann J, Rinaldi F, Debernardi P, Michalzik R. VCSELs with enhanced single-mode power and stabilized polarization for oxygen sensing. IEEE Photon Technol Lett 2005;17:2256–8.

[9] Yan Z, Lin H, Coldren A. Control of polarization phase offset in low lhreshold polarization switching VCSELs. IEEE Photon Technol Lett 2011;23:305–7.

[10] Li S, Guan B L, Shi G Z, Guo X. Polarization stable vertical-cavity surface-emitting laser with surface sub-wavelength gratings. Acta Phys Sin 2012;61:184208.

[11] Boutami S, Benbakir B, Leclercq J L, Viktorovitch P. Compact and polarization controlled 1.55 μm vertical-cavity surface-emitting laser using single-layer photonic crystal mirror. Appl Phys Lett 2007;91:071105.

[12] Ostermann J, Debernardi P, Jalics C, Kroner A, Riedl M, Michalzik R. Surface gratings for polarization control of single- and multi-mode oxide-confined vertical-cavity surface-emitting lasers. Opt Commun 2005;246:511–9.

[13] Arteaga M A, Unold H J, Ostermann J M, Michalzik R, Thienpont H, Panajotov K. Investigation of polarization properties of VCSELs subject to optical feedback from an extremely short external cavity—part I: theoretical analysis. IEEE J Quantum Electron 2006;42:89–101.

[14] Yu J, Chen Y, Cheng S, Lai Y. Temperature dependence of anisotropic mode splitting induced by birefringence in an InGaAs/GaAs/AlGaAs vertical-cavity surface-emitting laser studied by reflectance difference spectroscopy. Appl Opt 2013;52:1035–40.

[15] Yukio I, Toshio Y. Linear and nonlinear rotordynamics: a modern treatment with applications. 2nd ed.Wiley; 2012; 110–201.

[16] Coldren LA, Corzine SW, Mashanovich ML. Diode lasers and photonic integrated circuits. 2nd ed.. New Jersey: Wiley; 2012; 210–30.

[17] Haglund , Gustavsson J S, Bengtsson J, Jedrasik P, Larsson A. Design and evaluation of fundamental-mode and polarization-stabilized VCSELs with a subwavelength surface grating. IEEE J Quantum Electron 2006;42:231–40.

[18] Huang M C Y, Zhou Y, Chang-Hasnain C J. Single mode high-contrast subwavelength grating vertical cavity surface emitting lasers. Appl Phys Lett 2008;92:171108.